Open access • Journal Article • DOI:10.1051/RPHYSAP:01988002304060500

Creep and fracture of metals : mechanisms and mechanics — Source link

B.F. Dyson

Institutions: National Physical Laboratory

Published on: 01 Apr 1988

Topics: Creep, Dislocation creep and Diffusion creep

Creep and fracture of metals : mechanisms and mechanics

B.F. Dyson

Revue Phys. Appl. **23** (1988) 605-613 AVRIL **1988**, PAGE 605
Classification
Physics Abstracts
62.20

Creep and fracture of metals : mechanisms and mechanics

B.F. Dyson

Division of Materials Applications, National Physical Laboratory, Teddington, Middlesex, TW11 OLW, G.B.

(*Reçu le 24 juillet 1987, révisé le 21 janvier 1988, accepté le 22 janvier 1988*)

Résumé.- Les méthodes modernes ayant pour but l'amélioration du dimensionnement des pièces travaillant à haute température, nécessitent la prévision du comportement des materiaux dans des conditions proches de celles en service. Ce besoin a polarisé l'attention des ingénieurs sur le compréhension des phénomènes d'accumulation de dommage dans les alliages. La microstructure des métaux peut se dégrader par plusieurs mécanismes qui dépendent; (i) de la température; (ii) souvent de l'état de constrainte; et (iii) parfois de la composition chimque de l'environnement. Dans ce papier, quelques récents développements dans la modèlisation des processus d'endommagement sont rappelés. En particulier, l'emploi d'une seule variable d'état est évalué et on souligne le bénéfice potentiel d'utiliser deux variables d'état. Un système deux-barres a été utilisé pour quantifier certaines caractéristiques du fluage associées à la cavitation aux joints de grains, et a permis de démontrer le bon accord entre la théorie et les expériences. Un modèle pour l'endommagement de fluage associé à l'évolution des sous-structures de dislocations dans un super-alliage base-nickel a ensuite été développé et verifié expérimentalement.

Abstract.- Modern methodologies that aim to reduce conservatism in the design of components operating at high temperatures rely on accurate predictions of materials' behaviour in conditions relevant to those experienced in service. This requirement has focussed the attention of materials engineers on developing a quantitative understanding of damage-accumulation in engineering alloys. The microstructure of metallic materials can degrade by several mechanisms at rates that depend; (i) on temperature; (ii) often on stress level or state; and (iii) sometimes on the chemistry of the surrounding fluid environment. In this paper, some recent developments in the modelling of damage processes have been reviewed; in particular, the single state variable approach has been assessed and the potential benefits of using two state variables outlined. Also, a two-bar mechanical analogue has been used to quantify certain features of creep deformation associated with grain boundary cavitation and the close agreement between theory and experiment is demonstrated. A model for the creep damage associated with the evolution of the dislocation substructure in nickel-base superalloys has been developed further and experimental support for an unusual feature of the model has been demonstrated.

1. Introduction

In power generation, power propulsion and petrochemical plant, the main failure modes of key metallic components loaded for protracted periods at temperatures in excess of 500 °C are fracture, fatigue, excessive corrosion, excessive deformation and sometimes, wear. The evolving science of component design aims to minimise the risk of such failures (with their attendant economic penalties and sometimes danger to human lives) while still effecting a competitive design.

As far as creep deformation and fracture are concerned, a basic difficulty for the designer is that component geometries are often such that the stresses are not statically determinate but depend on the material-law relating strain, ϵ, or strain rate, $\dot{\epsilon}$, to stress, σ, and temperature, T. Simple design is elastic:

$$\sigma = E(T)\epsilon \qquad [1]$$

where the modulus, E, is a function of temperature. This leads to very conservative (ie cost-inefficient) designs because the calculated maximum stress is unnecessarily high: in service, this maximum stress is reduced by creep and its spatial position within the component also changes with time. More complicated design-procedures attempt to account for this stress redistribution, usually by assuming a "steady state" constitutive law of the form:

$$\dot{\epsilon} = \dot{\epsilon}_o \left[\frac{\sigma}{\sigma_o}\right]^n \qquad [2]$$

where $\dot{\epsilon}_o$ is a temperature-dependent creep parameter at the arbitrary normalising stress, σ_o, and n is a constant. Stationary state stress distributions can be calculated analytically for only a few component geometries and finite element methods are now being used increasingly for the more usual complicated shapes: the resultant stress fields can still lead to conservatism in design because Eq. 2 does not take into account the further stress redistribution that takes place during the tertiary creep period. The creep damage tolerance parameter, $\lambda = \epsilon_f/\dot{\epsilon}_i t_f$ (where ϵ_f is the fracture strain of a constant load uniaxial testpiece with initial stress,

σ_i, strain rate, $\dot{\epsilon}_i$, and lifetime t_f) is a measure of the potential effectiveness of this further stress redistribution since the lifetime, $t_{f,c}$, of a local region within a statically indeterminate component under a stress, σ_i, redistributed at a rate given by Eq. 2 is (1):

$$t_{fc} = \lambda t_f \qquad [3]$$

It has been estimated (2) that λ needs to be greater than 5-10 to extend local lifetimes sufficiently to justify the safe usage of upper bound estimates of component lifetimes, as given by Reference Stress Analyses.

Physically based modelling of materials behaviour aims to predict creep deformation and fracture lifetimes under the variable stress levels/states and thermal/fluid environments encounted in service: to be applied successfully to components, such modelling studies must also be able to predict λ. This paper reviews the state-of-the-art of physically based, predictive modelling of creep and creep fracture and in addition to providing new experimental evidence for creep constrained cavitation fracture, develops further a tertiary creep model for nickel-base superalloys.

2. Physically based models of material damage

2.1 *Single state variable approach.*

When metals and alloys are subjected to load at temperatures in excess of approximately 0.3 T_m, the trajectory of strain as a function of time usually exhibits three distinct stages called primary, secondary and tertiary creep. This simple characteristic, while providing a useful *operational* description of behaviour, hides the very important fact that creep can be caused by several micromechanisms operating together or in sequence. This would be unimportant technologically, were it not that engineers inevitably require extrapolations of laboratory data for use in design and these necessitate a mathematical description of creep. The usual empirical descriptions, including the new θ projection concept (3), cannot anticipate changes in mechanism and extrapolations can in principle be subject to considerable error. Creep data need to be extrapolated in four main ways: (i) to longer times; (ii) to conditions of variable load and temperature; (iii) to non uniaxial states of stress and (iv) to conditions of external fluid environments not readily achievable in the laboratory.

Lifetime is dictated by the mechanics of the various tertiary creep mechanisms and engineers use the phrase "creep damage" to describe the material degradation that occurs during this period. Continuum Creep Damage Mechanics (CDM) is a formalism that has been developed to describe damage accumulation (4-7) and the background to this approach will be presented before a discussion of the physics of models of material damage. The basic assumptions of CDM are that a single state variable, ω, can describe the microstructural state of the material adequately and that the evolution of damage with time causes the accelerating creep rate and failure. To enable extrapolations to conditions of variable load and temperature, two differential equations are required viz:

$$\dot{\epsilon} = f(\sigma, T, \omega,) \qquad [4]$$

$$\dot{\omega} = g(\sigma, T, \omega,) \qquad [5]$$

Integration of explicit forms of Eqs 4 and 5 as a coupled pair will produce the strain/time trajectory for any arbitrary history of load or temperature: the problem lies in determining explicit forms of these two equations. The engineering literature follows the suggestions of Kachanov (4) and Rabotnov (5) viz:

$$\dot{\epsilon} = \dot{\epsilon}_o \left[\frac{\sigma}{\sigma_o(1-\omega)} \right]^n \qquad [6]$$

$$\dot{\omega} = \dot{\omega}_o \left[\frac{\sigma}{\sigma_o(1-\omega)} \right]^m \qquad [7]$$

Thus damage is regarded as changing σ to a nett stress, $\sigma_{nett} = \sigma/(1-\omega)$ and $0 \leqslant \omega \leqslant 1$. Lifetime is found by integrating Eq 7 and usually, but not necessarily, taking the value unity for the damage at failure, ω_f. When m and ω_f are both independent of stress, it can be shown (8) that the integration yields Robinson's Life Fraction Rule for predicting lifetime under variable loading. Odquist and Hult (8) further demonstrated that the *necessary* and *sufficient* requirements for Robinson's Rule to predict lifetime under any arbitrary excursion of temperature and stress when a single state variable system operates, is that the damage rate, Eq 5, should be a separable function of σ, T and ω, ie:

$$g(\sigma, T, \omega) = h(\sigma) j(T) k(\omega) \qquad [8]$$

and that ω_f should be a constant. This leads to the conclusion that Kachanov's special description of damage as a nett section stress necessarily requires $k(\omega)$ to be a power law function of stress before Robinson's Rule can apply. For example, if $\dot{\omega} \propto \exp(B\sigma_{nett})$ then σ and ω cannot be separated and Robinson's Rule will not hold for histories of variable stress, *even though a single damage mechanism is operating*; a fact not apparently appreciated in the literature. These arguments suggest that Robinson's Rule is more likely to be applicable to histories of variable temperature than of variable stress and may explain why Remanent Life Procedures are best tackled using isostress rather than isothermal extrapolation procedures.

Kachanov's original model has been extended to include primary creep (6) and multiaxial stresses (7), when ω may then have to be treated as a tensor: it is thus a very powerful engineering design tool but suffers - as does any purely empirical model - from the inability to extrapolate beyond the stress levels/states, temperatures and testing environments contained in the database. Progress has recently been made by attempting to put creep damage within a physically-based CDM framework (9-11). In Table 1, creep damage is placed into three broad categories, each containing more than one mechanism. There is a certain arbitrariness in this categorisation and Ashby and Dyson (11) chose to use four categories rather than three, simply because damage due to environmental attack depends on section size and is therefore not a state variable. It should be noted that other damage mechanisms exist, for example the evolution of mechanical instabilities, but these have not yet been quantified. The three categories are described below.

Damage due to loss of external section.

This type of damage is a progressive increase in stress with time due to the decrease in cross sectional area, caused either by straining under conditions of constant load or because environmental attack produces a reaction product - usually oxide, sulphide or carbide - which spalls periodically after a critical strain has been reached (11).

Damage due to microstructural degradation.

Engineering alloys are often strengthened by a dispersion of precipitated particles which are unstable with respect to time and temperature and thus grow either competitively at constant volume fraction (Ostwald Ripening) or dissolve in favour of different, more stable, particles. This intrinsic instability of the particulate microstructure has led some researchers to believe that this is the *primary* cause of "damage" giving rise to the extensive period of tertiary creep found in nickel-base superalloys, certain low alloy ferritic steels and certain aluminium alloys. However, this has been shown not to be the case (12), at least for nickel-base superalloys at stresses well below the particle-cutting stress, and the proposal is that the 'damage' causing these extensive

periods of tertiary creep is due to the intrinsic instability of the dislocation substructure to deformation. The physical basis of the model summarised in Table 1 is given in section 4: for present purposes, it suffices to know that the parameter C characterises the importance of this mechanism.

Attempts have been made to model creep rate when an initial second-phase microstructure is gradually replaced by a more stable one - for example, one set of particles by another (9, 13) - so giving rise to sigmoidal curves when lifetime is plotted against stress: this case is not included in Table 1.

Damage due to loss of internal section.

It is now well established that intergranular fractures are caused by the nucleation and growth of holes (cavities) on grain boundaries. Two types of cavity distribution can be identified and are illustrated in Fig 1. These are (i) macroscopically uniform, which is the more usual or (ii) concentrated in a region contiguous with the external environment: this being prima facie evidence that the cavities are a consequence of attack by a chemical component(s) of the environment. In both cases, cavities are distributed non uniformly on the scale of the grain size; being on those grain boundaries predominantly perpendicular to the applied maximum principal tensile stress. The gradual accumulation of cavities contributes directly to fracture, but also causes an increase in the rate of creep. The minimum acceleration is when growth is "unconstrained" (10) - the holes simply increase the applied stress in proportion to their area fraction: while the maximum acceleration occurs when growth is "constrained" and the *effective* area fraction of holes can then become equal to the area fraction occupied by transverse boundaries in a uniaxially loaded system. A more detailed account of this concept is given in Section 3.

TABLE I: Creep damage categories and mechanisms

CREEP DAMAGE CATEGORY	MECHANISM	DAMAGE PARAMETER ω	DAMAGE EVOLUTION RATE $\dot{\omega}$	STRAIN RATE $\dot{\epsilon}$	$C_m = \dot{\epsilon}_i t_f$ ($\omega_f = 1$)	ϵ_f	$\lambda = \frac{\epsilon_f}{C_m}$
LOSS OF EXTERNAL SECTION	Uniform Straining Under constant load (11)	$1 - \frac{A}{A_i}$	$\dot{\epsilon}_i \left[\frac{1}{1-\omega}\right]^{n-1}$	$\dot{\epsilon}_i \left[\frac{1}{1-\omega}\right]^{n}$	$\frac{1}{n}$	∞	∞
	Periodic Failure of Corrosion-product (11)	$\frac{2x}{R}$	$\dot{\omega}_{ic} \left[\frac{1}{1-\omega}\right]^{n}$	$\epsilon_i \left[\frac{1}{1-\omega}\right]^{n}$	Not applicable to large ω		
MICROSTRUCTURAL DEGRADATION	Thermal coarsening of particles (11, 12)	$1 - \frac{s_i}{s}$	$(1-\omega)^{\frac{4}{3}} K'$	$\dot{\epsilon}_{ip} (1+K''\omega)^{n}$	∞	∞	∞
	Instability of the dislocation substructure	$1 - \frac{\rho_i}{\rho}$	$C\dot{\epsilon}_i$	$\dot{\epsilon}_i (1-\omega)^{-1}$	$\frac{1}{C}$	∞	∞
LOSS OF INTERNAL SECTION	Environmentally-induced damage (11, 15)	$\frac{2x}{R}$	$\frac{2K}{R^2 \omega}$	$\dot{\epsilon}_i \left[\frac{1}{1-f\omega}\right]^{n}$	Not applicable to large ω		
	Cavity growth by grain boundary diffusion (10, 11)	$\left(\frac{r}{l}\right)^2$	$\dot{\epsilon}_{ig} \frac{d}{2l\omega^{\frac{1}{2}}} \frac{\ln 1/\omega_i}{\ln 1/\omega}$	$\dot{\epsilon}_{ig} \frac{\ln 1/\omega_i}{\ln 1/\omega}$	$\sim \frac{4}{3}\frac{1}{d}$	$\sim \frac{8}{3}\frac{1}{d}$	~ 2
	Cavity nucleation with creep-constrained growth (14)	F	$\dot{\omega}_{in} \left[\frac{1}{1-k\omega}\right]^{m}$	$\dot{\epsilon}_i \left[\frac{1}{1-k\omega}\right]^{n}$	$\frac{\dot{\epsilon}_i [1-(1-k)^{n+1}]}{(n+1)\dot{\omega}_{in}}$	$\frac{k\dot{\epsilon}_i}{\dot{\omega}_{in}}$	~ 2

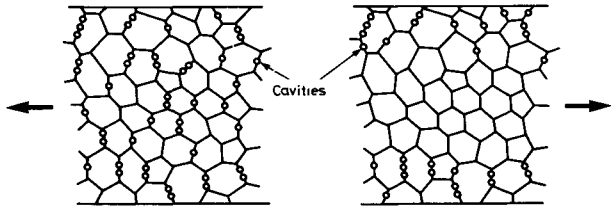

Fig 1: Illustrating the two types of cavity distribution.

For each mechanism in Table 1, a damage parameter has been defined which has both a physical identity and the Kachanov characteristic of varying between zero and unity. In each case, the damage parameter leads to expressions for $\dot{\epsilon}$ and $\dot{\omega}$ that are usually of the Kachanov type (Table 2 defines the symbols used in Table 1). When a set of equations for $\dot{\epsilon}$ and $\dot{\omega}$ is integrated under constant temperature and loading conditions, expressions are obtained for; (i) the Monkman-Grant parameter $C_m = \dot{\epsilon}_i t_f$; (ii) the strain at failure, ϵ_f, and therefore; (iii) the creep damage tolerance parameter $\lambda = \epsilon_f / C_m$. In Table 1, only those values at $\omega_f = 1$ are given and, as such, are upper bound values for each mechanism acting alone. Four interesting features are displayed in Table 1.

First, the Monkman Grant constant C_m for nickel-base superalloys of high ductility is of the order 0.02 (these materials damage through instability of the dislocation substructure with $C \triangleq 50$ (12, 14, 16)), while Type 316 stainless steels with high ductility exhibit a C_m of order 0.2: these materials damage because of increasing nett stress when creep occurs under constant load and n is typically 5. The practical consequence of the operation of the dislocation substructure mechanism is that upper-bound lifetimes of nickel-base superalloys are one order of magnitude less than those found with a 316 stainless steel of the same 'creep strength' - as conventionally measured by the value of the minimum creep rate.

Secondly, the definition of the damage parameter for the dislocation substructure mechanism is different from that used previously (14, 16), in order to conform to Kachanov's constraint that $0 \leqslant \omega \leqslant 1$.

Previously, damage was defined (16) as:

$$s = \ln(\rho/\rho_i)$$

which made the damage unbounded. These different definitions of damage and damage rate are easily related by the transformations:

$$\omega = 1 - \exp(-s)$$

$$\dot{\omega} = \exp(-s)\dot{s}$$

Thirdly, the damage parameter for environmental attack, 2x/R, is an approximation; thus loss of internal or external section can be calculated only when $\omega << 1$ and so values of C_m, ϵ_f and λ at $\omega_f = 1$ are not included in Table 1. For loss of external section by environmental attack, C_m and ϵ_f are given, for $\omega << 1$ by (11):

$$C_m = \frac{R}{n+2}\left[\frac{\epsilon^*\dot{\epsilon}}{K_p}\right]^{\frac{1}{2}}\left[1 - (1-\omega_f)^{\frac{n+2}{2}}\right] \quad [9]$$

$$\epsilon_f = \frac{R}{n-2}\left[\frac{\epsilon^*\dot{\epsilon}_i}{K_p}\right]^{\frac{1}{2}}\left[\left[\frac{1}{1-\omega_f}\right]^{\frac{n-2}{2}} - 1\right] \quad [10]$$

For loss of internal section by environmental attack, the equivalent equations are (11,15):

$$C_m = \frac{R^2\dot{\epsilon}_i\omega_f^2}{4K} \quad [11]$$

TABLE II: Definition of symbols used in Table I

A, A_i	:	cross-sectional area of a cylindrical bar; subscript i denotes the initial section.
$\dot{\epsilon}_i = \dot{\epsilon}_o(\sigma_i/\sigma_o)^n$	:	creep rate at time = 0 of a power-law creeping solid under a uniaxial stress σ_i.
$C_m = \dot{\epsilon}_i t_f$	:	Monkman-Grant constant.
ϵ_f	:	strain at failure.
$\lambda \equiv \epsilon_f/C_m$	:	creep damage tolerance parameter.
R	:	radius of cylindrical bar.
x	:	depth of corrosion-product or of internal environmental-attack.
ϵ^*	:	critical strain required to fracture an external film of corrosion product and reduce its load-carrying capacity to zero.
K_p	:	parabolic rate constant for growth of external corrosion-product.
$\dot{\omega}_{ic} \equiv \frac{2}{R}\left[\frac{K_p\dot{\epsilon}_i}{\epsilon^*}\right]^{\frac{1}{2}}$	:	the damage rate at time = 0 due to the strain-induced, periodic failure of an external film of corrosion product.
s, s_i	:	spacing between second phase particles; subscript i denotes initial value.
K'	:	rate constant in particle-coarsening law; $s^3=s_i^3(1+K't)$.
$\dot{\epsilon}_{ip} \equiv \dot{\epsilon}_o\left[\frac{\sigma-\sigma_{pi}}{\sigma_o}\right]^n$	:	creep rate at time = 0 of a power-law creeping solid under constant stress, σ, with threshold stress, σ_{pi}.
$\sigma_{pi} = \frac{\alpha\mu b}{d_p}$	:	initial, local climb-controlled Orowan stress.
μ	:	shear modulus.
b	:	Burgers vector.
α	:	a constant.
K"	:	$\sigma_{pi}/(\sigma-\sigma_{pi})$.
ρ, ρ_i	:	dislocation density; subscript i denotes initial value.
$C \equiv k/b$	:	defined in Eq 43.
K	:	rate constant for internal oxidation.
$f \equiv 1 - \left[\frac{\dot{\epsilon}_{om}}{\dot{\epsilon}_{op}}\right]^{\frac{1}{n}}$	:	a measure of the creep strength of the zone of environment attack.
$\dot{\epsilon}_{om}$	:	creep rate in undamaged matrix at stress σ_o.
$\dot{\epsilon}_{op}$	:	creep rate in environmentally-attacked matrix at stress σ_o.
r	:	cavity radius.
2l	:	intercavity spacing.
d	:	grain size
$\dot{\epsilon}_{ig} \equiv \dot{\epsilon}_i\,\varphi_o\,\frac{2l}{d\ln 1/\omega_i}$	:	initial creep rate when creep is primarily due to cavity growth by stress-directed diffusion.
$\varphi_o \equiv \frac{2D_b\delta\Omega}{kTl^3}\,\frac{\sigma_o}{\dot{\epsilon}_o}$	:	a dimensionless material property.
δ	:	grain boundary width.
D_b	:	grain boundary diffusivity.
F	:	fraction of grains containing a cavitated transverse boundary.
$k \triangleq \frac{1}{3}$	:	fractional area occupied by transverse boundaries.
$\dot{\omega}_{in}$	:	initial cavitation damage rate.

$$\epsilon_f = \frac{\dot{\epsilon}_i R^2}{2K}\left[\frac{1}{n-1}\left\{\left[\frac{1}{1-f\omega_f}\right]^{n-1} - 1\right\} - \frac{1}{n-2}\left\{\left[\frac{1}{1-f\omega_f}\right]^{n-2} - 1\right\}\right] \quad [12]$$

The fourth and final point concerns the approximations inherent in the single state variable approach and the need to appreciate its limitations. The approximations revolve primarily around the use of ω_f = constant (usually unity) as a failure criterion, without due regard for the physical processes involved. This can easily be illustrated by reference to the particle-coarsening damage mechanism, where the use of $\omega_f = 1$ as a failure criterion leads to values of C_m, ϵ_f and λ approaching infinity. Taken literally, this would imply that this mechanism would never control lifetime, which is clearly of little value. In reality, a second failure mechanism intervenes at finite (and variable) values of the particle coarsening damage parameter $1 - s_i/s$ and leads to finite values of C_m, ϵ_f and λ.

2.2 *CDM with two damage variables*

A two state variable approach is required in order to overcome the inadequacies of CDM outlined in the previous paragraph, but little attention has been paid to the problems this uncovers, particularly with regard to the potential for synergy between the two damage processes. Formally, synergy is accounted for by the equation-set:

$$\begin{aligned} \dot{\epsilon} &= \dot{\epsilon}\ (\sigma\ T\ \omega_1\ \omega_2) \quad (a)\\ \dot{\omega}_1 &= \dot{\omega}_1\ (\sigma\ T\ \omega_1\ \omega_2) \quad (b)\\ \dot{\omega}_2 &= \dot{\omega}_2\ (\sigma\ T\ \omega_1\ \omega_2) \quad (c) \end{aligned} \quad [13]$$

The problems arise when deriving explicit forms of the equations: the simplest approximation is to assume that ω_2 has little influence on $\dot{\epsilon}$ and $\dot{\omega}_1$, so that the equations given in Table 1 remain valid. Thus

$$\begin{aligned} \dot{\epsilon} &= \dot{\epsilon}\ (\sigma\ T\ \omega_1) \quad (a)\\ \dot{\omega}_1 &= \dot{\omega}_1\ (\sigma\ T\ \omega_1) \quad (b)\\ \dot{\omega}_2 &= \dot{\omega}_2\ (\sigma\ T\ \omega_1\ \omega_2) \quad (c) \end{aligned} \quad [14]$$

Physically, this means that the effect of the second damage variable is to fix the value of ω_1 at fracture ie, the only influence is to change ϵ_f and not to change the trajectory of strain as a function of time.

An even simpler approximation along these lines was used by Ashby and Dyson (11) in order to estimate the effect of the necking instability on C_m, ϵ_f and λ due to damage caused by the increase in nett section stress in a constant load test. The inclusion of this modification results in substantial changes to the values of ϵ_f and λ given in Table 1 viz:

$$\epsilon_f \triangleq \frac{2}{n-1} \quad [15]$$

$$\lambda \triangleq \frac{2n}{n-1} \quad [16]$$

The value of C_m is still well approximated by the Hoff (17) relationship:

$$C_m \triangleq \frac{1}{n} \quad [17]$$

A proper treatment of necking still awaits an evolution equation for the growth of tensile necks - currently, only numerical solutions exist (18) - but Fig 2 demonstrates how well this simple treatment applies to a Type 316 stainless steel: the measured value of ϵ_f is 42% while that calculated from Eq 15 is 40%; the measured value of λ is 2.7 while that calculated from Eq 16 is 2.4; and the measured value of C_m is 0.15 while that calculated from Eq 17 is 0.17.

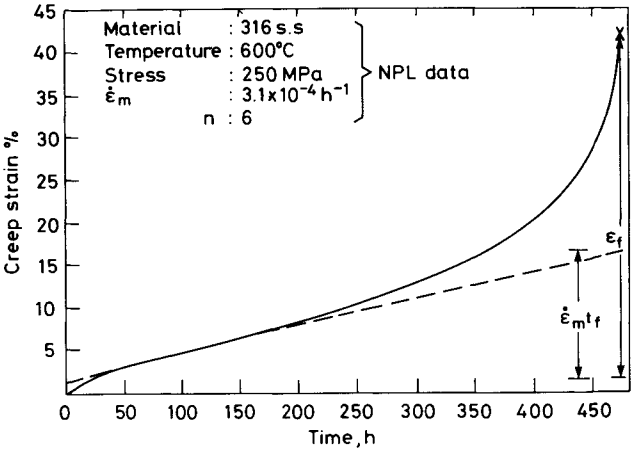

Fig 2: Creep strain as a function of time for Type 316 stainless steel.

Dyson and Gibbons (14) have proposed an approximate equation-set with two damage variables to explain the behaviour of nickel-base superalloys with ductilities ranging from less than 1% to greater than 20% (beyond which extensive necking occurs in these alloys). Under conditions of constant temperature and stress, the relationship between creep strain and time is predicted to be:

$$\epsilon_\sigma = -\frac{1}{C + n/3\epsilon_f} \ln\left[1 - (C+n/3\epsilon_f)\dot{\epsilon}_i t\right] \quad [18]$$

Creep under conditions of constant or variable load were treated by introducing a third damage variable. Again, analytical solutions are easily obtained for isothermal creep under constant load, viz:

$$\epsilon_\ell = -\frac{1}{C + n(1+1/3\epsilon_f)} \ln\left[1 - \{C + n(1+1/3\epsilon_f)\}\ \dot{\epsilon}_i t\right] \quad [19]$$

Eq 19 is plotted in Fig 3 as a function of the dimensionless parameter $\dot{\epsilon}_i t$, using C = 50 and n = 5 for a number of different values of ϵ_f (full lines) and using C = 0, n = 5 (dashed lines). C is a material parameter which characterises the instability with respect to strain of the dislocation substructure and whose possible physical origins are discussed in Section 4. There are two points of special importance in Fig 3. The first is that for alloys with a stable dislocation substructure (C = 0), t_f is directly proportional to ϵ_f - until t_f approaches the Hoff limit - and thus λ is a constant (approximately equal to 2, Table 1). The second is that when an alloy has an unstable dislocation substructure (for example, C = 50), t_f is not very sensitive to changes in ϵ_f (and thus $\lambda \propto \epsilon_f$) provided $\epsilon_f \geqslant n/3(C+n)$ whereas t_f becomes increasingly proportional to ϵ_f when $\epsilon_f \leqslant n/3(C+n)$. These characteristics are clearly displayed in Figs 4 and 5.

It should be noted that two damage variables will always be required to characterise creep and fracture when tertiary creep is dominated by the operation of any of the first five mechanisms listed in Table 1. Only when tertiary creep and fracture are caused by the *same* mechanism (the last two in Table 1) will a single state variable accurately reflect behaviour.

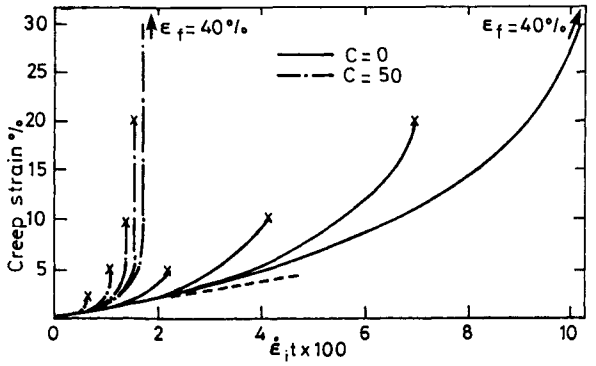

Fig. 3 Predicted values of creep strain as a function of the parameter $\dot{\epsilon}_i t$ for intrinsically stable (C=0) and unstable C=50) alloys at various levels of ductility.

3. Two-bar modelling of creep and fracture

Grain boundary cavities are always distributed non-uniformly on the scale of the grain size and sometimes also on a macroscale, as illustrated in Fig 1. In either case, this non-uniformity leads to internal stress patterns which reflect the scale of the non-uniformity. For the case of macro-uniform, micro-non-uniform cavity distribution, Fig 1(a), the corresponding effect on the strain (strain-rate) response can be modelled approximately using a two-bar analogue, Fig 6. Bar α represents the fraction, $(1-\omega)$, of material not containing cavities, while bar β represents the fraction, ω, that does. The applied stress is required by equilibrium to redistribute according to:

$$\sigma = \sigma_\alpha(1-\omega) + \sigma_\beta\omega \qquad [20]$$

where σ_α and σ_β denote the internal stresses.

The strain rates $\dot{\epsilon}_\alpha$, $\dot{\epsilon}_\beta$ in each bar are given by:

$$\dot{\epsilon}_\alpha = A\left[\frac{\sigma_\alpha}{\sigma_o}\right]^n + B\left[\frac{\sigma_\alpha}{\sigma_o}\right] + \frac{\dot{\sigma}_\alpha}{E} \qquad [21]$$

$$\dot{\epsilon}_\beta = A\left[\frac{\sigma_\beta}{\sigma_o}\right] + B\left[\frac{\sigma_\beta}{\sigma_o}\right] + B'\left[\frac{\sigma_\beta - \frac{2\gamma}{r}}{\sigma_o}\right] + \frac{\dot{\sigma}_\beta}{E} \qquad [22]$$

where E is Young's Modulus and A, B, B' are temperature-dependent creep rates at stress σ_o, representing matrix dislocation creep, diffusion creep and creep due to cavity growth by stress-directed diffusion respectivly.

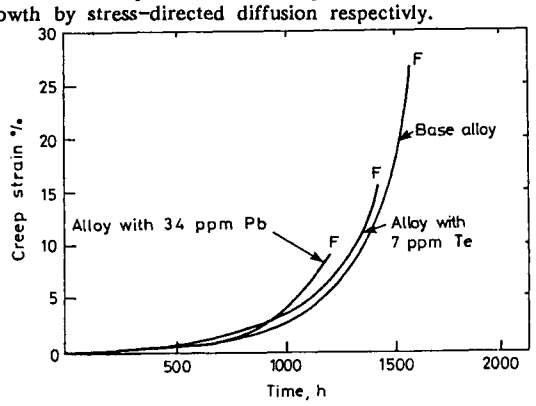

Fig 4: Creep strain as a function of time for three specimens of Nimonic 105 with different levels of trace elements; tested at 815 °C and 232 MPa. (Ref. 14). Tertiary creep in this alloy is dominated by the instability of the dislocation substructure which leads to t_f being insensitive to ϵ_f.

When diffusion creep and cavity creep are controlled by grain boundary transport, suitable approximations for B and B' are given by (19, 10):

$$B = \frac{148\ D_b\delta\Omega\sigma_o}{kT\pi d^3} \qquad [23]$$

$$B' = \frac{4\ D_b\delta\Omega\sigma_o}{kT\ell^2 d\ln(1/f_h)} = \frac{\pi}{37\ \ln(1/f_h)}\left[\frac{d}{\ell}\right]^2 B \qquad [24]$$

D_b is the grain boundary diffusivity; δ the grain boundary width; Ω the atomic volume; d the grain size and f_h the fractional area of a grain boundary facet occupied by cavities of spacing 2ℓ, radius r and surface tension, γ.

The extent of stress redistribution, its effect on creep rates and the time constant for steady state clearly depend on ω and on the relative values of A, B and B'. Two technologically important bounds will be considered. The first is the trivial case when the strain rate due to cavity growth is very much *less* than that due to either matrix or diffusion creep. Stress redistribution is then negligible, cavity growth is termed "unconstrained" and the macroscopic creep rate is given by the sum of $A(\sigma/\sigma_o)^n$ and $B(\sigma/\sigma_o)$. This situation becomes dominant at higher stresses and/or lower temperatures. The largest stress redistribution occurs when the strain rate due to cavity growth is very much *greater* than that due to either matrix or diffusion creep: it is more likely to become dominant at higher temperatures and service levels of stress. For a simple illustration, consider the case when diffusion creep is very much faster than matrix creep: Eq's 21 and 22 then become:

$$\dot{\epsilon}_\alpha = B\left[\frac{\sigma_\alpha}{\sigma_o}\right] + \frac{\dot{\sigma}_\alpha}{E} \qquad [25]$$

$$\dot{\epsilon}_\beta = (B+B')\left[\frac{\sigma_\beta}{\sigma_o}\right] + \frac{\dot{\sigma}_\beta}{E} \qquad [26]$$

where the initial cavity radius is assumed to be large enough to permit $\sigma_{i\beta} = \sigma >> 2\gamma/r_i$ - the subscript i denotes the value of r at the nucleation stage.

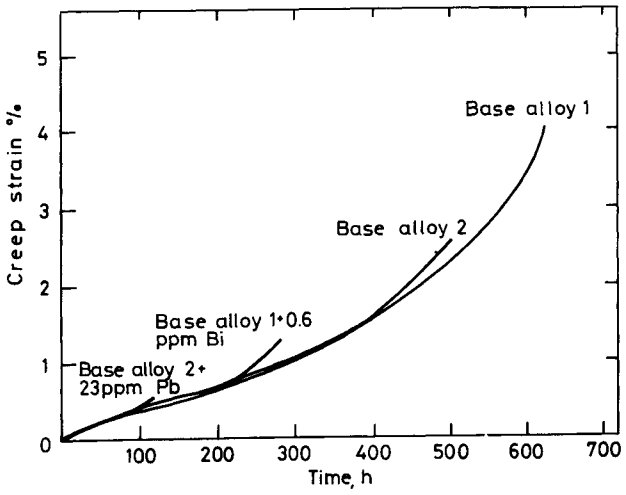

Fig 5: Creep strain as a function of time for four specimens of conventionally cast Mar M002 with different levels of trace elements; tested at 850 °C and 350 MPa (Ref. 14). Tertiary creep in this alloy is dominated by cavitation which leads to t_f being directly proportional to ϵ_f.

Eqs. 25 and 26 can be solved by noting (i) $\dot{\epsilon}_\alpha = \dot{\epsilon}_\beta$ and, since σ = constant, (ii) that:

$$\dot{\sigma}_\beta = -\left[\frac{1-\omega}{\omega}\right]\dot{\sigma}_\alpha$$

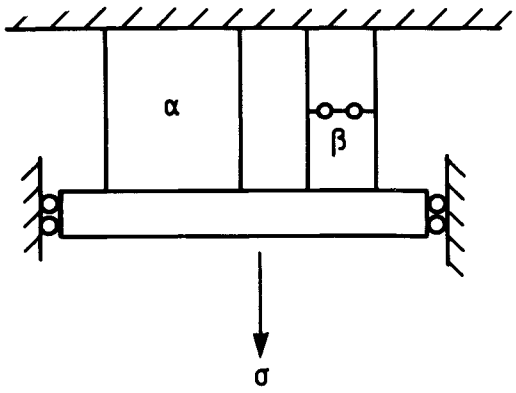

Fig 6: Two-bar mechanical analogue for creep of a material containing grain boundary cavities.

Thus

$$\sigma_\alpha = \frac{B'\sigma}{B + B'(1-\omega)}\left[\left[\frac{B}{B'} + 1\right] - \omega \exp\left\{\frac{E[B+B'(1-\omega)]}{\sigma_o}\right\} t\right] \quad [27]$$

The stresses will approximate those at the stationary state when the term in the exponential equals unity. Thus, when $B' >> B$, maximum stress redistribution will occur after time:

$$\tau = \left[\frac{\sigma_o}{E}\right]\frac{1}{B'(1-\omega)} \quad [28]$$

with stresses

$$\sigma_{\alpha s} \triangleq \frac{\sigma}{1-\omega} \quad [29]$$

$$\sigma_{\beta s} \triangleq 0 \quad [30]$$

Cavity growth is then termed 'creep constrained' and has an associated volumetric growth rate:

$$\dot{\nu} = (2\ell^2)dB\left[\frac{\sigma}{1-\omega}\right] \quad [31]$$

When matrix creep is much faster than diffusion creep, then Eqs. 28 - 30 still apply but stationary state strain rates and $\dot{\nu}$ contain the term $(\sigma/1-\omega)^n$.

The 2-bar model of stress redistribution due to cavity growth therefore predicts that under matrix creep constrained conditions, the initial creep rate is:

$$\dot{\epsilon}_{in} = B'\left[\frac{\sigma}{\sigma_o}\right] \quad [32]$$

which decays to a stationary state value after time τ, Eq. 28, given by:

$$\dot{\epsilon}_s = A\left[\frac{\sigma}{\sigma_o(1-\omega)}\right]^n \quad [33]$$

During this transient period, the recoverable strain accumulated is given by:

$$\epsilon_t = \frac{\omega}{1-\omega}\frac{\sigma}{E} \quad [34]$$

Equations 32 and 33 differ significantly with respect to changes in stress and temperature and this presents the experimentalist with an opportunity to test the predictions of this simple 2-bar model. Changes in temperature should reveal an activation energy equal to that for grain boundary diffusion for initial creep rates but secondary creep rates should exhibit an activation energy at least twice that value. Fig. 7 displays creep data for the alloy Nimonic 80A prestrained 15% at room temperature (20); values of initial creep rate and secondary creep rate at a stress of 460 MPa are plotted as a function of the reciprocal absolute temperature. The activation energy for secondary creep is determined from the slope to be 382 kJ mole^{-1}, while that for the initial creep rate is very much lower. The activation energy for grain boundary diffusion is in dispute for nickel and its alloys: the experimental value of 115 kJ mole^{-1} (21) being very much at variance with the predicted value of ~ 150 kJ mole^{-1}, given by Brown and Ashby (22) for this class of metal. Both values have been used to generate slopes through three of the points in Fig. 7. Either slope is consistent with the 2-bar model prediction and both suggest that the test at 750°C is not in the creep constrained cavity growth region, since an extrapolation of either line would intercept the secondary creep rate line at a temperature below 750°C and so violate the conditions outlined above for the applicability of creep constrained growth. Further evidence that the test at 750°C was unconstrained is that

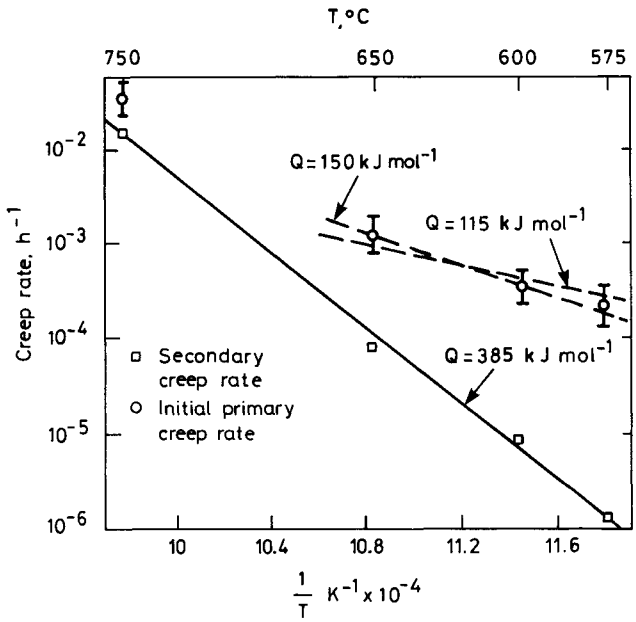

Fig 7: Initial creep rate and secondary creep rate data for Nimonic 80A prestrained 15% at room temperature prior to testing at 460 MPa. The error bars reflect the difficulty of measuring initial creep rates.

the failure strain was >6%, whereas the other three exhibited failure strains of approximately 2%. The transition between constrained and unconstrained growth of cavities is characterised by a marked increase in strain to failure: Fig. 8 demonstrates this for a CrMoV steel, heat treated to simulate the heat affected zone in a weldment. The transition locus between constrained and unconstrained cavity growth can be calculated in an approximate manner (23) but requires more material property data than are available with this particular data-set.

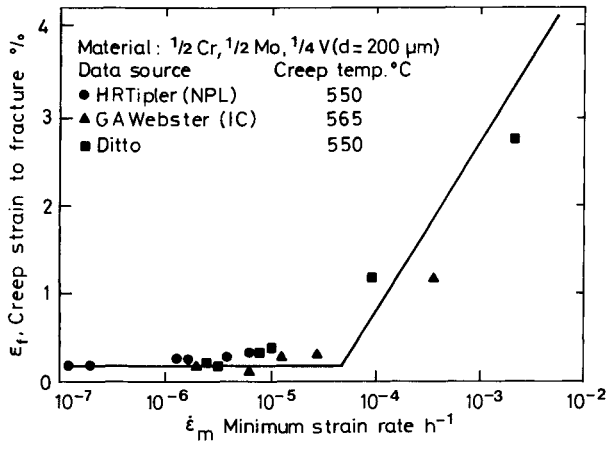

Fig 8: Creep strain at fracture plotted as a function of minimum strain rate for a ½Cr ½Mo ¼V steel with a grain size of 200 μm. Two data-sources are used. Creep constrained cavity growth occurs at strain rates below $5 \times 10^{-5} h^{-1}$, while unconstrained growth occurs above that value.

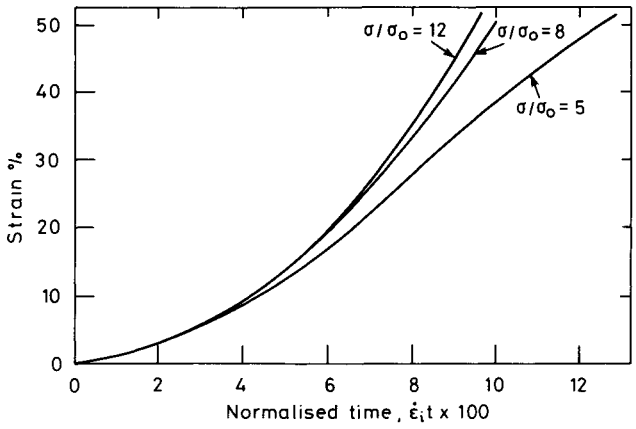

Fig 9: Predicted values of creep strain as a function of $\dot{\epsilon}_i t$; derived from Eq's 39 - 41.

4. Mechanistic basis of creep models for superalloys

Nickel-base superalloys of high ductility - greater than approximately 10% strain at fracture - are characterised by the fact that most of the strain (>90%) is accumulated during the tertiary stage of creep, as is most of the lifetime. Dyson and McLean (12) argued, from experimental data and theory, that coarsening of the γ' particles was not the cause of this extended period of tertiary creep, at least for applied stresses well below the mean value of the particle cutting stress, σ_p, which is the operative flow mechanism for these alloys in their normal heat treated condition. At stresses approaching the mean particle-cutting stress (perhaps $\geq \sigma_p/2$), there is evidence in the literature (24) that particle coarsening is an *additional* mechanism of tertiary creep, but still not the primary one. Thus, in the context of section 2, a completely accurate description of tertiary creep covering all stresses below σ_p, requires two state variables, even in the absence of damage due to fracture processes. However, this section will be concerned only with the primary mechanism of creep in these alloys and develops further an idea proposed previously (11, 12): if correct, it should adequately reflect the behaviour of these materials at service stress levels. The proposed mechanism is that *all* dislocations are free to move at a velocity, v, controlled by osmotic climb, viz:

$$v = 2v_o \sinh \left[\frac{K\sigma_e}{T\sigma_o} \right] \qquad [35]$$

v_o and K are constants and σ_o is a normalising stress defined by:

$$\sigma_o = \alpha\mu b \sqrt{\rho_i}$$

σ_e is the effective stress responsible for climb, viz:

$$\sigma_e = \sigma - \alpha\mu b \sqrt{\rho} \qquad [36]$$

Creep rate is given by:

$$\dot{\epsilon} = \rho b v \qquad [37]$$

The strain/time trajectory requires evolution equations for ρ and v: $\dot{v}$ can be obtained by differentiating Eq 35 and $\dot{\rho}$ by assuming that dislocations multiply during climb by the mechanism proposed by Taylor for glide, viz:

$$\dot{\rho} = \delta v \rho \qquad [38]$$

where δ is the dislocation breeding coefficient. Constitutive and damage evolution equations suitable for numerical integration can be obtained from Eq's 35 - 38 by defining two damage parameters, ω_1 and ω_2 in the Kachanov manner:

$$\omega_1 = 1 - \frac{\rho_i}{\rho}$$

$$\omega_2 = 1 - \frac{v}{v_i}$$

Thus

$$\dot{\epsilon} = \dot{\epsilon}_i \left[\frac{1 - \omega_2}{1 - \omega_1} \right] \qquad [39]$$

$$\dot{\omega}_1 = C' \dot{\epsilon}_i (1-\omega_1)(1-\omega_2) \qquad [40]$$

$$\dot{\omega}_2 = D[1 - G(1-\omega_2)^2]^{\frac{1}{2}} \frac{\dot{\omega}_1}{(1-\omega_1)^{3/2}} \qquad [41]$$

where

$$\dot{\epsilon}_i = \rho_i b v_i$$

$$D = \frac{v_o}{v_i} \frac{K}{T}$$

$$G = \left[\frac{v_i}{2v_o} \right]^2$$

$$C' = \delta / \rho_i b$$

In deriving Eq's 39 - 41, δ was assumed constant: with $\dot{\omega}_2 = 0$, Eq's 39 and 40 combine to given the linear strain softening model (16).

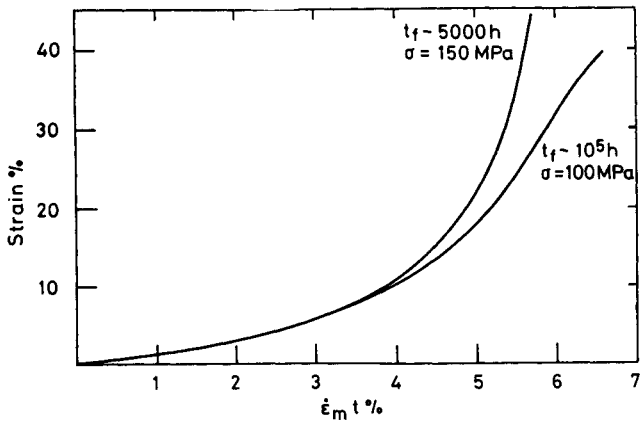

Fig 10: Creep strain in torsion as a function of $\dot{\varepsilon}_m t$; demonstrating the onset of sigmoidal creep at the lower stress.

If it is assumed that $\delta = k\rho$, where k is a constant, then Eq 40 is replaced by:

$$\dot{\omega}_1 = C\dot{\varepsilon}_i(1-\omega_2) \quad [42]$$

and $C = k/b$ [43]

When $\dot{\omega}_2 = 0$, Eq's 39 and 42 combine to give the exponential strain softening used in a previous publication (16) and in Table 1.

Eq's 39 - 41 have been integrated numerically to yield creep strain as a function of the dimensionless parameter $\dot{\varepsilon}_i t$ for various values of normalised stress σ/σ_o, using the following values for the other parameters: $\alpha = 1/2$; $\mu = 8 \times 10^4$ MPa; $b = 2 \times 10^{-10}$ m; $\rho_i = 10^{12}$ m^{-2}; $\dot{\varepsilon}_o = 5 \times 10^{-14}$ s^{-1}; K = 240; T = 1100K; C' = 50. The results are plotted in Fig. 9 but, for clarity, only three values of σ/σ_o are presented. For present purposes, the important point to note is the sigmoidal shape of the creep curve at $\sigma/\sigma_o = 5$: the degree of sigmoidal behaviour increases with decreasing values of σ/σ_o and is simply a consequence of the decreasing dislocation velocity with increasing strain. Such behaviour has never been reported for nickel-base superalloys but Fig. 10 shows some data taken from NPL files of the creep of Nimonic 80A in torsion: the data were published in another form by Dyson and McLean (25). Signs of sigmoidal behaviour can be seen in the 100 MPa test and an unusual linear behaviour can be seen at large strains in the 150 MPa test: at higher stresses, the normal continuously increasing strain rate with strain was always observed. Although by no means conclusive, the results in Fig. 10 add confidence to the view that tertiary creep in these alloys is a consequence of the mechanism outlined in this section.

Sigmoidal shapes of creep curve are well known in the literature and a theory along the lines presented here has been published for glide-controlled creep by Alexander and Haasen (26). The unusual features of nickel-base superalloys are that creep is climb controlled and that the point of inflection in the creep curve is at least an order of magnitude greater than reported for other materials.

5. Acknowledgements

The author expresses his gratitude to Dr Ana Barbosa for writing the computer program to solve Eq's 39 - 41 and to Dr T B Gibbons for constructive comments on the manuscript.

6. References

1. F.A. Leckie and D.R. Hayhurst (1978) Creep of Engineering Materials. Ed. C.D. Pomeroy. Mech. Eng. Pub. Ltd. London p.111.

2. I.N. Goodall, R.D.M. Cockroft and E.J. Chubb (1975) Int. J. Mech. Sci, 17 351.

3. R.W. Evans, J.D. Parker and B. Wilshire (1983) Recent Advances in Creep and Fracture of Eng. Mats. and Structures, Eds. B. Wilshire and D.R.J. Owen, Pineridge Press.

4. L.M. Kachanov (1958). Izv. Akad. Nauk. SSSR. No.8 p.26.

5. Yu. N. Rabotnov (1969) Proc. XII IUTAM Congress Stanford, Eds. Hetenyi and Vincenti, Springer p.342.

6. J. Hult (1974) On Topics in Applied Continuum Mechanics Eds. J.L. Zeman and F.Ziegler, Springer p.137.

7. F.A. Leckie and D.R. Hayhurst (1977) Acta Metall, 25, 1059.

8. F.K.G. Odquist and J. Hult (1961) Ark. Fys, 19, 379.

9. C.J. Bolton, B.F. Dyson and K.R. Williams (1980) Mat. Sci. and Eng. 46, 231.

10. A.C.F.Cocks and M.F. Ashby (1982) Progress in Mat. Sci. 27, 189.

11. M.F. Ashby and B.F. Dyson (1984) Advances in Fracture Research Eds. S.R. Valluri et al. Vol. 1. Pergamon Press. p.3.

12. B.F. Dyson and M. McLean (1983) Acta. Metall, 31, 17.

13. J.K.L. Lai (1986) Stainless Steels '84, Inst. of Metals.

14. B.F. Dyson and T.B. Gibbons (1987) Acta Metall. 35, 2355.

15. B.F. Dyson and S. Osgerby (1987) Mat. Sci. and Tech. in press.

16. J.C. Ion, A. Barbosa, M.F. Ashby. B.F. Dyson and M. McLean (1986). The Modelling of Creep for Engineering Design - I. NPL Report DMA A115.

17. N.J. Hoff (1953) J. Appl. Mech. 20, 105.

18. V. Tvergaard (1987) Acta. Metall. 35, 923.

19. R.L. Coble (1963) J. Appl. Phys. 34, 1679.

20. NPL unpublished data.

21. A.R. Wazzan (1965) J. Appl. Phys. 36, 3596.

22. A.M. Brown and M.F. Ashby (1980) Acta. Metall. 28, 1085.

23. B.F. Dyson and M.S. Loveday (1980) Engineering Aspects of Creep Inst. of Mech. Engs. London paper C205/80, 61.

24. R.A. Stevens and P.E.J. Flewitt (1979) Mater. Sci. and Engng. 37, 237.

25. B.F. Dyson and D.McLean (1977) Met. Sci. 11, 37.

26. H. Alexander and P. Haasen (1968) Solid State Physics 22, 27.